Northumbria Research Link

Deep learning artificial intelligence framework for sustainable desiccant air conditioning system: Optimization towards reduction in water footprints

Rasikh Tariq [a,b,*], Muzaffar Ali [c], Nadeem Ahmed Sheikh [d], Muhammad Wakil Shahzad [e,**], Ben Bin Xu [e]

[a] Facultad de Ingeniería, Universidad Autónoma de Yucatán, Av. Industrias No Contaminantes por Anillo Periférico Norte, Apdo. Postal 150, Cordemex, Mérida, Yucatán, Mexico
[b] Tecnológico Nacional de México/IT de Mérida, Departamento de Sistemas y Computación, Mérida, Mexico
[c] Mechanical Engineering Department, University of Engineering and Technology, Taxila, Pakistan
[d] Mechanical Engineering Department, Faculty of Engineering & Technology, International Islamic University, Islamabad, Pakistan
[e] Mechanical & Construction Engineering Department, Northumbria University, Newcastle Upon Tyne NE1 8ST, United Kingdom

ARTICLE INFO

ABSTRACT

Desiccant evaporative cooling systems pave the path towards energy and environmental sustainability in buildings especially; however, the direct evaporative coolers in such configurations result in high water consumption. The application of modern computational intelligence tools, including artificial intelligence and meta-heuristic optimization algorithms, can improve the operational comprehension of desiccant cooling systems while addressing the minimization of total water footprints with the maximization of the cooling capacity. The contribution/**objective** of this research is to address the gaps in understanding through the application of deep learning, genetic algorithm, and multicriteria decision analysis applied to a desiccant cooling system working under real transient experimental conditions of a building located in Austria. Within the **methodology**, calibrated, experimental, and validated data monitoring system displaying the real desiccant-enhanced cooling system is adapted to generate a set of input-output data sets. The set of data includes ambient temperature, ambient humidity, regeneration temperature, supply airflow rate, and return airflow rate yielding the cooling capacity and total water footprints of the system. The **results** of deep learning algorithm using an artificial neural network have suggested that the architectures 5-[6]-[6]-1 and 5-[12]-[12]-1 are the best to accurately predict the cooling capacity and total water footprints with a coefficient of determination of 0.98856 and 0.99246, respectively. Secondly, the "white-box model" of the deep learning algorithm is used to develop a digital twin model which helps in the replication of the earlier experimental conditions. The optimization results have suggested that the optimized total water footprints are 45.17 kg/h with a system of 3.32 tons of refrigeration. These optimal values are found in the best combination of design variables in which the ambient temperature is 28 °C, ambient relative humidity is 52.0%, supply airflow rate is 2.13 kg/s, and regeneration flow rate is 2.35 kg/s, and the regeneration temperature is 70.0 °C. It is concluded that the application of data-driven models can extend the interpretation of desiccant cooling systems and can participate in its performance enhancement.

1. Introduction

As the concerns of global warming and temperature rise are turning into reality, nations across the globe have tried to develop a unified front to tackle the biggest challenge to the existence of living beings on this planet. In modern & developing urbanized centers of the human population, the demand for air conditioning [1,2] is rising steeply as it is consuming as high as 70% of prime energy sources in countries situated in MENA regions. Such consumption of electrical power to keep built-up structures is highly unsustainable. Therefore alternatives are proposed based on several techniques and one famous method, proven in commercial units as successful, is desiccant-based evaporative cooling [3]. This is not a newer idea for air cooling, as evaporation is known to be a

---

<div style="border:1px solid">

Nomenclature

Letters

CC	Cooling capacity of the supply air, tons
$c_{p,\,air}$	Specific heat of air, kJ/kg.^{o}C
$\dot{m}_{supply\ air\ flow\ rate}$	Mass flow rate of the supply air, kg/s
$\dot{m}_{return\ air\ flow\ rate}$	Mass flow rate of the return air, kg/s
RH_{amb}	Ambient relative humidity, %
Q_{supply}	Supply flow rate, kg/s
$Q_{regeneration}$	Regeneration flow rate, kg/s
R^2	Coefficient of Determination
TWF	Total water footprints, kg/h
$TWF_{supply\ side}$	Total water footprints on the supply side, kg/h
$TWF_{return\ side}$	Total water footprints on the return side, kg/h
$T_{supply\ air\ temperature}$	Supply air temperature, ^{o}C
$T_{ambient}, T_{amb}$	Ambient air temperature, ^{o}C
T_{reg}	Regeneration temperature, ^{o}C

Symbols

$\omega_{supply\ air}$	Absolute humidity of the supply air, kg/kg
$\omega_{exit\ of\ desiccant\ wheel}$	Absolute Humidity at the exit of the desiccant

wheel, kg/kg

$\omega_{room\ return\ air}$	Absolute Humidity of the room in the return air, kg/kg
$\omega_{exit\ of\ return\ humidifier}$	Absolute Humidity at the exit of the return humidifier, kg/kg

Abbreviations and acronym

ANN	Artificial neural network
BRA	Bayesian regularization algorithm
DEC	Desiccant evaporative cooling system
EER	Energy Efficiency Ratio
LMA	Levenberg-Marquardt algorithm
MLP	Multilayer perceptron
MSE	Mean-square error
MAPE	Mean absolute percentage error
MENA	Middle East and North Africa
MIMO	Multiple Input and Multiple outputs
RMSE	Root-Mean-Square-Error
SCGA	Scaled Conjugate Gradient algorithm
TOPSIS	The Technique for Order of Preference by Similarity to Ideal Solution
XAI	Explainable Artificial Intelligence

</div>

source of cooling air for generations [4–11]. To overcome the challenges of latent as well as sensible load handling, improving air quality in humid/tropical regions, working below wet-bulb barrier [12], utilizing return air energy [13], renewable integration [14], open cycle with refrigeration [15] benefits (especially in the COVID-19 pandemic), etc. are some of the talking points of the desiccant based evaporative cooling technology.

With the growing concern on the working control, especially of the sub-systems such as desiccant wheel and regeneration heat source, of the open-cycle cooling methods used in desiccant-based evaporative cooling, there is a dire need to look at the performance matrix and find a method to bring the multi-system into a predictive controllable or even intelligent regime. This is particularly important as opposed to air-tight building-based controls. For instance, humidity control is more intrinsic here in the desiccant system as separate load handling [16] is essential, unlike the vapor compression cycle which is not greatly influenced in terms of the control system. While the benefits are counted with high regard for desiccant-based systems including high EER (Energy Efficiency Ratio) [17], a great deal of concern is also mentioned regarding the water consumption of these systems as it involves evaporative cooling devices (both direct as well as indirect coolers). This has a direct impact on the water consumption of these systems especially if employed at a large scale in desert/hot climatic conditions which usually have scarce water resources, especially in the global south.

Moreover, the operational part of the desiccant air cooling systems can involve several air cycle configurations such as ventilated mode working, Dunkle cycle, etc. There is extensive literature informing the need and working of these cyclic configurations in different working conditions/climatic zones. Intelligent switching is direly needed so that the same set of equipment (the majority of items are the same in most configurations) can be automatically tuned to work for best-suited performance indicators. This is of high importance from the perspective of manufacturers as well. These units can only be excellent sells and prove alternatives to conventional technologies if they are adaptive in nature.

The use of intelligence in the predictive and automatic control of air cooling, both active as well as passive, using data-driven models is not a new area. Many regressive, machine learning [18], data-driven [19], and predictive control strategies have been proposed in the literature. These models and strategies mainly aim to make the system or its components responsive and controllable to the varying conditions, input

parameters, and system dynamics. Therefore, intelligence in the control system of the HVAC systems is essential for optimal performance. Various techniques are being implemented for the efficient performance of building HVAC systems like energy modeling and Model Predictive Control (MPC) [20]. The application of artificial neural network (ANN) for predicting the performance of solid desiccant cooling systems was found feasible [21]. Independent temperature/humidity control strategies were implemented for precooled desiccant-based evaporative cooling systems to ensure room comfort with less energy. The new control strategies were developed based on proportional and fuzzy+-proportional techniques which resulted in 20% energy savings compared to the traditional ON/OFF control [22]. In desiccant air conditioning systems, a desiccant wheel and direct/indirect evaporative cooler are the key components. A high-low (H-L) control strategy on regenerative indirect evaporative coolers caused 11.3% less energy consumption annually [23]. In addition, a year-round optimization method of L/H was also proposed by considering energy consumption, thermal comfort, and switch frequency. The lowest annual energy consumption of RIEC is observed when L/H is about 0.3 [24]. Annually, IEC with variable speed fans consumes 50.0% less energy than that on-off fans by applying proportional–integral (PI) law based variable speed technology for accurate temperature control in an IEC system [25]. Regarding desiccant wheel control, multiple regression and machine learning models of rotary desiccant wheel were developed for performance prediction. It was determined that predictive power of the MLR models increases as the degree of equation increases and cross terms are added [26]. Moreover, an adaptive neuro-fuzzy inference system with artificial neural network fuzzy logic was implemented to predict the exit parameters of desiccant coated heat exchangers. It was analyzed that ANFIS–AI tool with ANN fuzzy logic can be used as a reference AI tool for the efficient design and performance prediction, analysis, and optimization of any heat exchanger [27].

Goldsworthy et al. [28] solved the heat and mass transfer equations for combined solid desiccant-indirect evaporative cooling and concluded that a regeneration temperature of 70 °C, supply/regeneration flow rate of 0.67, and an indirect cooler secondary/primary flow rate of 0.1 can give the optimal performance. Hung-Yi et al. [29] developed and validated a numerical model including the heat and mass transfer for the rotary desiccant wheel and included the factors like ambient temperature, ambient humidity, air flow rate, the rotational speed of the wheel, wheel split, and regeneration airstream temperature

to offer the optimized control strategies for the operation of rotary desiccant wheel installed for a hotel building. Wang et al. [30] used a simulation method including a parametric and optimization study on a novel transient air dehumidifier to meet a constant energy supply with multi-stage desiccant plates. Rayegan et al. [31] also proposed an optimization based upon a dynamic simulation for a solar-assisted desiccant cooling system but it was also integrated with a ground source heat exchange. The results have suggested that the system can not provide thermal comfort in extremely humid regions with high regeneration temperatures and the integration with ground source heat exchange can significantly decrease the regeneration temperature. Zhang et al. [32] focused on the optimization through exergy destruction analysis of a liquid desiccant dehumidification system and obtained an exergy efficiency improvement to around 4%. Ou et al. [33] applied a model-based optimization strategy for liquid desiccant cooling and dehumidification and suggested an energy consumption reduction of over 12.49% through the adaption of the optimal control strategy. Tu et al. [34] considered various air handling units under different ambient humidity ratios along with various other variables in the desiccant air cooler to suggest two control strategies under winter ambient conditions. The authors obtained a satisfactory rate of over 95%. Boudjabi et al. [35] conducted parametric analysis including multiobjective and single-objective optimization and concluded that the unique airflow configuration of a combined parallel-regenerative cooler is higher in drier climates to report a cooling capacity improvement by 5% at the cost of water consumption increment of about 40%. Motaghian et al. [36] have suggested optimum and effective purge angles for different dimensionless dehumidification angles, rotational speeds, number of transfer units, and regeneration temperature in desiccant wheels. Chen et al. [37] combined photovoltaic and thermal solar power, dehumidification, and active cooling along with the development of a component scale mathematical model of a solar-driven liquid desiccant air conditioning system especially targetting extremely hot and humid climates. Bouchaala et al. [38] used a multiobjective particle swarm optimization algorithm to display the Pareto optimality of conventional adsorption ventilated cooling systems and concluded that the use of a purge zone during the optimization process can improve the cycle performance.

While the effort on the sub-system/component control has merits. However, the overall behavior of the system under varying configurational parameters, ambient/input conditions, resources, and air conditioning requirements is much more complicated owing to Multiple Inputs and Multiple outputs (MIMO). MIMO includes air entering and returning to the system, water sprayed in humidifiers [39], and heat input to heaters while the thermal comfort in terms of temperature and humidity control to the air-conditioned space are major outputs. The 'black-box' modeling approach may serve the whole desiccant system, albeit requiring realizability. Moreover, the dynamic variations in the ambient and operational parameters (for all inputs including ambient air, water, and energy/power especially utilizing renewable sources) require a dynamic model. Thus, as suggested by the literature review, it can be concluded that the current optimization studies have not focused on the usage of direct experimental data of a working building to offer digital twinning i.e. empirical modeling, and multiobjective optimization especially to focus on the reduction of water footprints of the desiccant air conditioning systems.

Data-driven model development leads to the generation of a 'digital twin', which acts as a responsive decision-making tool. Several examples of digital twinning can be seen in the energy sector [40]. Here using an actual experimental dataset of a working building [41], is taken for the generation of the digital twin. Initially, a black box-based approach is used for the model to develop its performance matrix and validate its work. However, upon realization, the model is optimized for a set of operations conditions of the system which otherwise would not have been generated using the digital twin. Ensuring that the realizable operating conditions, where the system shall be responding and operational, are used for optimal space search; the 'while box' model

approach is introduced here to ensure a realizable decision/recommendation for multi-objective optimal working. This realizable recommendation is primarily the initial ingredient of XAI (explainable Artificial Intelligence) which is introduced in the forthcoming sections.

2. System description

In the current work, a solid desiccant evaporative cooling system (DEC) of a real building [41] located in Vienna, Austria is considered. The key components of the system include a silica-gel-based desiccant wheel, a heat wheel along with two direct humidifiers i.e. supply humidifier and return humidifiers which are the main sources of water consumption. The overall DEC system is equipped with numerous sensors continuously measuring all significant parameters at the individual component as well as at the system levels. Two data monitoring systems, Siemens DESIGO Insight [41] and JEVis [41] are used for data recording from all sensors. The system schematic with instrumentation is shown in Fig. 1 (a). The process starts with the increase of temperature of ambient air with dehumidification (process 1–2). During the dehumidification, the process air loses moisture and increases temperature. Afterwards, the temperature of this air is reduced sensibly through the heat wheel (process 2–3) with subsequent addition of moisture using a direct humidifier (process 3–4). The regeneration side includes series of processes involving humidification (process 5–6), sensible heating (process 7–8) and desiccant wheel regeneration (process 8–9) as shown in Fig. 1(b). Key aspects of technical design data of the main components of the installed DEC system are given in Table 1.

In this system, each humidifier is equipped with four sensors, two at the inlet and two at the outlet, each pair measuring temperature and relative humidity at both locations. K-type thermocouple are used for temperature measurement having range from 0 to 200 °C, accuracy of 0.3% and with resolution of 0.1 °C. Whereas, resistive air humidity sensors are employed that have range of 0 to 100% for relative humidity, and 0–18 g/kg for humidity ratio with resolution of 1% RH and accuracy of ± (3% of reading +1% RH). These sensors are coupled with data acquisition for continuous measurements of temperature and air humidity. Consequently, the data set of six selected days consists of air temperature and relative humidity along with the rotation speed of the spray pump. The monitoring setup of both humidifiers is shown in Fig. 1 (c). In the actual monitoring set-up, the water mass flow rate from the spray pump was not measured. The water mass flow rate depends on the inlet conditions of the air in terms of its temperature, absolute humidity, and mass flow rate along with the rotational speed signal of the spray pump.

3. Method

The system under consideration is shown schematically in Fig. 1 (a). The desiccant evaporative cooling system is integrated with multiple components to provide the air-conditioned space with the flow rate of conditioned air. This system involves two main sides, the process side, and the return side respectively. The process side takes the ambient air which passes through the desiccant wheel to remove excessive moisture. The desiccant wheel is a rotating water-absorbing pad that is continually recharged using the return side air. The next component is the heat recovery wheel which transfers the heated air, the air while getting moisture removed is heated, to the return side. This recovery of energy assists in the recharging of the desiccant wheel. The next component in the cyclic configuration of Fig. 1 (a) is the suction fan, which sucks the air through the first two components. The air, after heated and moisture removed, is passed through the evaporative cooler/supply humidifier to bring the temperature and humidity of the air to the required temperature and relative humidity through water spray for supplying to an air-conditioned room.

The return side uses the return air from the air-conditioned room while controlling the temperature and humidity of the room. The first
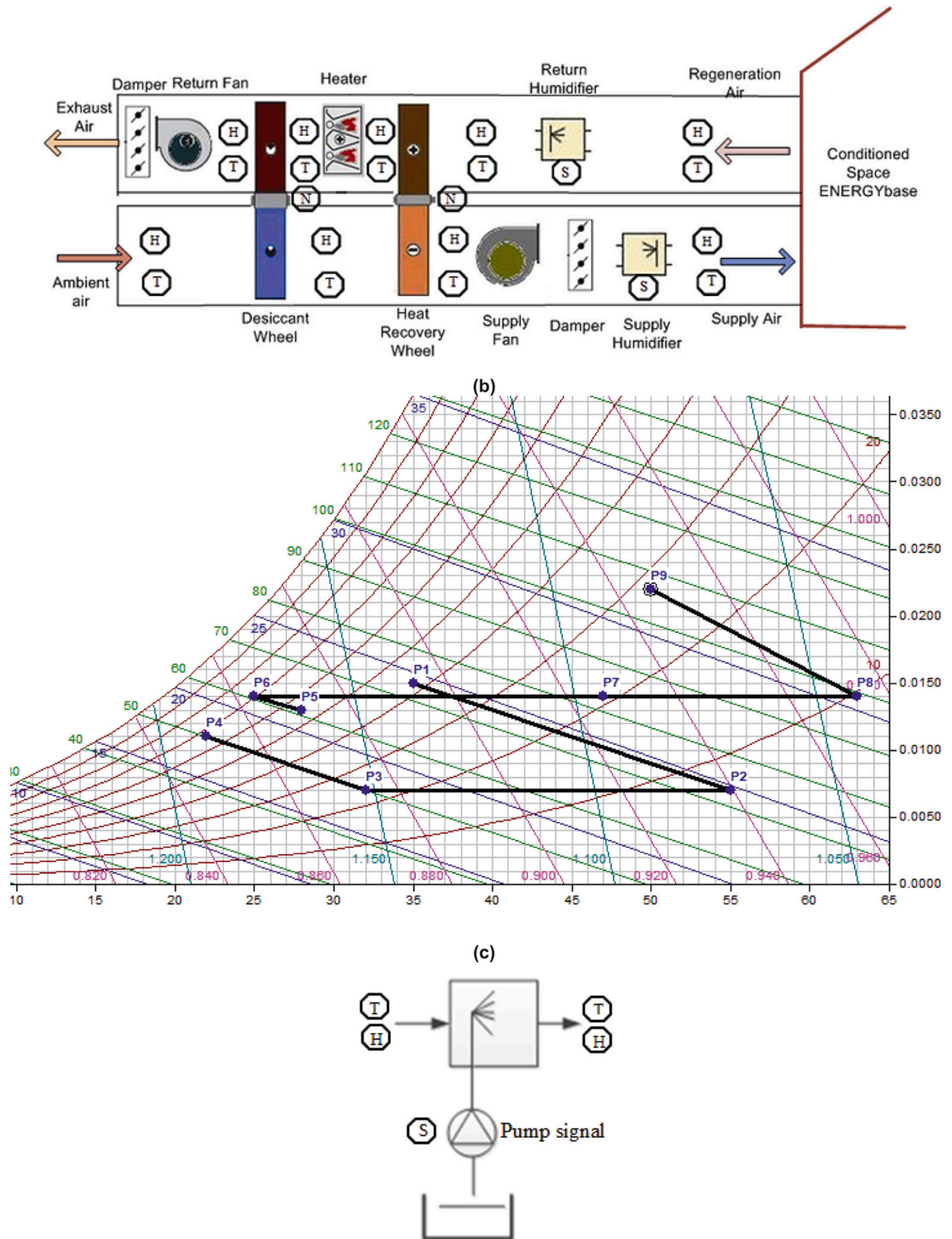
Fig. 1. The considered desiccant evaporative cooling system: (a) schematic diagram with instrumentation, (b) psychrometric representation of processes, (c) data sensors for direct evaporative supply and return humidifiers.

component is the additional moisture addition before passing it on to the recovery wheel which heats up the air through heat transmission from the process side. The next stage is desiccant wheel discharging which usually takes place at a temperature greater than 70 °C. The additional heaters are installed to get the required heat energy for the air to

recharge the desiccant wheel. While the whole process is driven by the return side suction fan assisting the flow to be maintained. In the whole process, two important parameters are noted that rate the overall performance of the desiccant system. Namely, the cooling capacity of the system in terms of the amount of heat it can remove (measured

Table 1

Component design parameters of the system [41].

No.	DEC component design parameter	Details or design value
1	**Desiccant wheel**	Model SECO 1770, Klingenburg
	Air volume flow rate (m³/h)	8240
	Adsorbent	LiCl
	Wheel diameter (m)	1.77
	Wheel depth (m)	0.45
	Pressure drop (Pa)	164
	Wheel rotation speed (rph)	20
	Ambient air (°C / %)	32 / 40
	Supply air (°C / %)	46.9 / 12
	Regeneration air (°C / %)	70 / 10
	Exhaust air (°C / %)	55.1 / 20
2	**Heat wheel**	ModelRRS-P-16-18-1770-400, Klingenburg
	Air volume flow rate (m³/h)	8240
	Wheel diameter (m)	1.77
	Wheel depth (m)	0.4
	Wheel rotation speed (rpm)	10
	Pressure drop (Pa)	119
	Effectiveness	0.8
	Outdoor air (°C / %)	45 / 14
	Supply air (°C / %)	31.24 / 29
	Regeneration air (°C / %)	28 / 85
	Exhaust air (°C / %)	41.62 / 40
3	**Supply and return spray humidifiers**	Robatherm
	Air volume flow rate (m³/h)	8240
	Saturation efficiency (%)	90
	Dehumidification capacity (g/kg)	4.4
	Water flow rate (m³/h)	4.0
	Pump power (kW)	0.8
	Pressure drop (Pa)	235
	Supply air (°C / %)	32 / 33
	Exhaust air (°C / %)	21.26 / 89
4	**Supply and return fans**	RH 45C
	Air volume flow rate (m³/h)	8240
	Pressure drop (Pa)	600
	Power (kW)	4.3

conventionally in tons of air conditioning) as shown in eq. (1); while the second and equally important index is the total water consumed in humidification process both at the process as well as return sides. The total water footprint is measured and shown in eq. (2). The supply and return sides of water footprints are separately shown as well as eqs. (3) and (4) respectively.

$$\text{Cooling capacity (tons)} = \dot{m}_{\text{supply air flow rate}} \times c_{p,air} \\ \times \left(T_{\text{supply air temperature}} - T_{\text{ambient}} \right) \times 0.284345 \tag{1}$$

$$\text{TWF} = \text{TWF}_{\text{supply side}} + \text{TWF}_{\text{return side}} \tag{2}$$

$$\text{TWF}_{\text{supply side}} = 3600 \left(\omega_{\text{supply air}} - \omega_{\text{exit of desiccant wheel}} \right) \times \dot{m}_{\text{supply air flow rate}} \tag{3}$$

$$\text{TWF}_{\text{return side}} = 3600 \left(\omega_{\text{room return air}} - \omega_{\text{exit of return humidifier}} \right) \times \dot{m}_{\text{return air flow rate}} \tag{4}$$

In total two system performance indicators are identified and evaluated here. It is to be noted that the equations from (1) to (4) are generic thermodynamics performance indicators. The cooling capacity is

evaluated using mass flow rate, specific heat, and temperature difference. The factor 0.284345 is multiplied by the cooling capacity to get the units in tons of refrigeration. The water footprints on each side (supply and return side) are evaluated just through a generic mass (expressed in the form of 'humidity') balance where the difference of absolute humidity is multiplied by its appropriate mass flow rate.

4. Results and discussion

The results section includes a detailed interpretation of the deep learning model for the system including its operation on ventilation as well as re-circulation modes. The variation in the input parameters and the performance of the system in achieving thermal comfort are related to the range of variations. In addition, to thermal comfort, the water footprint on the air conditioning system is equally important as the demand for water for mass-scale utilization of desiccant-based cooling systems can impact scarce freshwater resources.

One key ingredient of the analysis present here is the evaluation of system performance in terms of achieving thermal comfort and the set of optimal input parameters ensuring it. However, this is constrained by the total water usage in the system to achieve the required temperature and humidity levels. This is directly linked with the usefulness of desiccant-based air cooling systems which claim to handle sensible and latent loads separately. The use of the desiccant-based system with direct or indirect evaporative coolers has a larger water footprint than conventional air cooling devices such as vapor compression or cryogenics. However, it offers merits in terms of separate load handling which can be mechanically more efficient. Nevertheless, the success of such desiccant-based evaporative cooling technology is directly linked to the water usage it will require especially in water-scarce regions of the globe. Here the linkage is established as multi-objective function optimization linking both thermal comfort as well as water footprint, while both have different requirements often countering/opposing each other. For instance, for a hot desert climate, the thermal comfort (both in terms of sensible as well as latent loads) shall be demanding water for air cooling and humidification despite the scarce availability of fresh/drinkable water in those regions. While in tropical conditions, the requirement for thermal comfort can be a great deal of removals of ambient moisture which shall be requiring higher temperatures for recharging the desiccant wheel. Thus in all conditions, water usage or removal is key to this air conditioning technology.

4.1. Statistical explanation of the data

The data selected for the desiccant system at hand is actual operational data for seven selected days during the month of July. The data includes a variety of input, process, monitoring, and output variables while operating in a daily routine. The data is time-averaged for an interval of 05 min, while the actual data is recorded each minute, to avoid any unnecessary fluctuation, which indicates a local/temporal peak/fluctuation only. Amongst the parameters recorded at all the input/output of each component in the desiccant system as shown in Table 2, primarily temperature and humidity, the selected system inputs and outputs are separated. These parameters are external, independent, and uncorrelated parameters that can impact the system alone or in

Table 2

Basic statistical details and characteristics of the design variables and the performance indicators.

Characteristic	Name of the variable	Symbol	Unit	Minimum value	Maximum value
Design variable 1	Ambient temperature	T_{amb}	°C	21.28	36.76
Design variable 2	Ambient relative humidity	RH_{amb}	%	13.71	100
Design variable 3	Regeneration temperature	T_{reg}	°C	21.3	80.66
Design variable 3	Supply flow rate	Q_{supply}	kg/s	0.10	2.70
Design variable 5	Regeneration flow rate	$Q_{regeneration}$	kg/s	0.021	2.78
Performance indicator 1	Cooling capacity	CC	tons	0.029	8.51
Performance indicator 2	Total water footprints	TWF	kg/h	0.39	60.78

combination with other parameters. These 05 parameters include the ambient temperature and relative humidity of the air, the regeneration temperature of the air, the flow rate at the supply side, and the regeneration side flow rate. These flow rates, ambient conditions, and regeneration temperature independently influence the cooling capacities and performance of the desiccant system while getting the required indoor conditions ensuring thermal comfort (i.e. cooling capacity) which is one output parameter/performance indicator. The other performance indicator is the water consumption by the system. The independent parameters and performance indicators are listed in Table 2 indicating the maximum and minimum values as seen in the actual data series.

Moreover, the model development focuses on the input-output of the complete system, which includes a number of sub-systems or components. Each component has its own characteristic; however, the model developed here uses the overall system input and maps it with the desired output along with its utility budget including heat requirements as well as water consumption. Therefore, the inputs of the complete system are considered here for the sake of the realizable model development. The input parameters and response parameters are well and diversely populated as highlighted in Fig. 2(b). The correlations amongst each of the input and output parameters are also included in the detailed parameter-to-parameter subplots shown in Fig. 2(b). It clearly indicates that some of the parameters such as ambient temperature and relative humidity are well varied while the regenerative temperature requirements fluctuate as the ambient condition on the

water content changes in the system. The flow rates of the system are not very well distributed in terms of the plot on the histogram. This indicates the system flow rates are somewhat steady and unperturbed. While the cooling capacity and total water footprint, show desired variability, which indicates that the system is fairly non-linear in its operability in different operating conditions. Moreover, the input parameters do not indicate any correlation, which means that the parameters are independent and can influence the system independently. On the other hand, the output parameters are not linearly linked as observable from Fig. 2 (b). These identifications are extremely important for data-driven modeling, optimization, and learning processes. The data seems suitable for extensive realizable development of system response characteristics which can be generalized upon learning and tuning techniques.

4.2. Deep learning neural network modeling of cooling capacity and water resource consumption

The developed experimental setup can mimic the real physical performance of the building-integrated desiccant cooling system, and it is desired to comprehend its optimal characteristics. This brings the need for the generation of an alternative surrogate, otherwise called a "digital twin", model of the data obtained from the experimentation procedure. The idea is to apply the data engineering model to replicate the actual experimental procedure with the purpose to find the operational optimality. In simple words, digital twin models are mathematical replications of the actual physical procedure which are developed under a set of
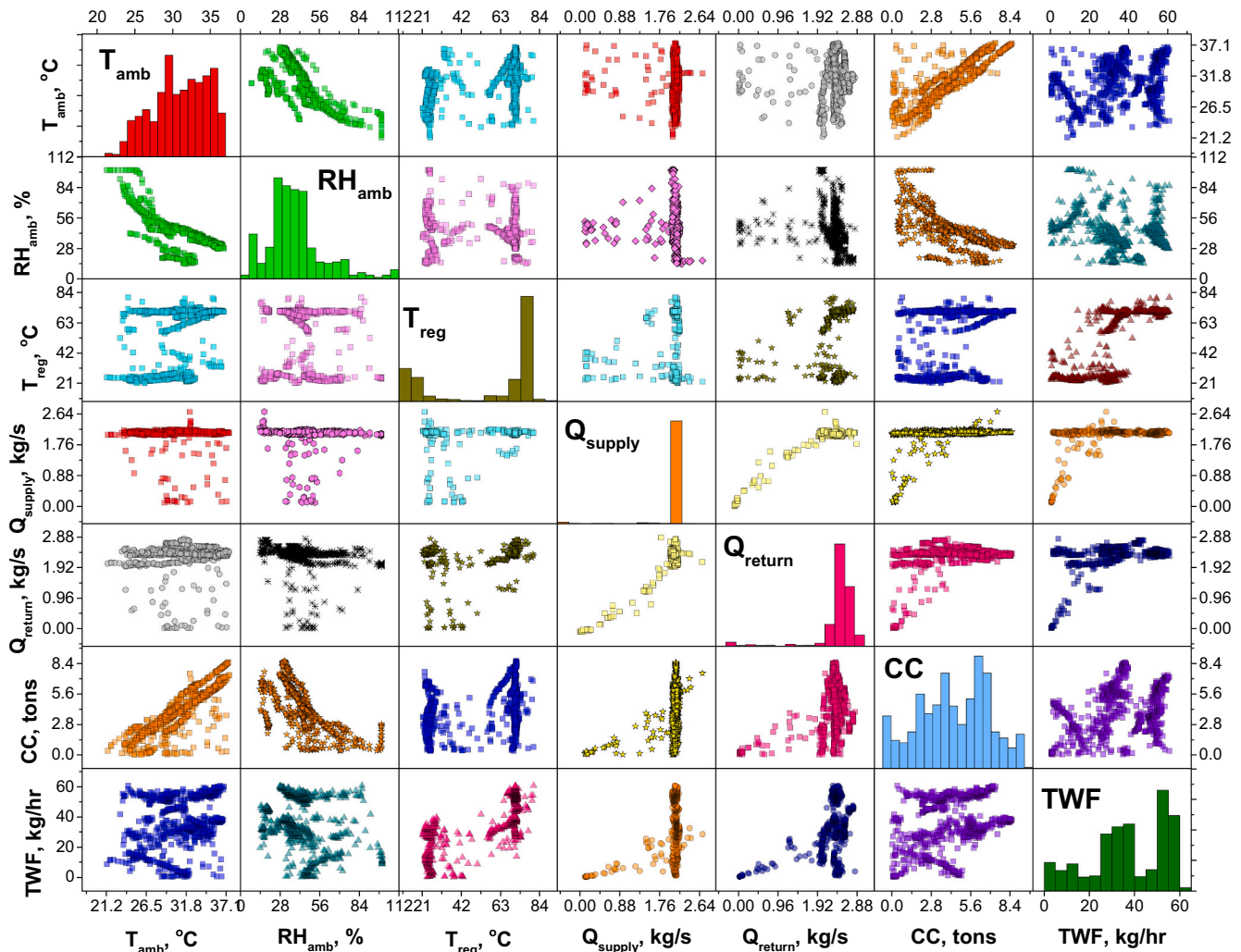

Fig. 2. Scatter matrix of the input-output data including the statistical distribution of the data.

Table 3
Selection of the most suitable ANN architecture for cooling capacity and total water footprints.

No.	Architecture	R^2	RMSE	MSE	MAPE
Cooling capacity					
1	5-[6]-1	0.97866	0.1027	0.0106	0.0848
2	5-[8]-1	0.98406	0.1296	0.0079	0.0889
3	5-[10]-1	0.98047	0.0983	0.0097	0.2249
4	5-[20]-1	0.98744	0.0797	0.0063	0.1563
5	**5-[6]-[6]-1**	**0.98856**	**0.0754**	**0.0057**	**0.0290**
6	5-[8]-[8]-1	0.97974	0.1023	0.0105	0.0972
7	5-[10]-[10]-1	0.98231	0.0946	0.0090	0.3728
Total water footprints					
1	5-[6]-1	0.95821	0.6192	0.3834	3.3792
2	5-[8]-1	0.95221	0.6268	0.3929	3.2451
3	5-[10]-1	0.96991	0.6305	0.3976	2.8177
4	5-[20]-1	0.97334	0.6382	0.4072	2.8767
5	5-[6]-[6]-1	0.97664	0.6305	0.3975	3.3042
6	5-[8]-[8]-1	0.98648	0.6448	0.4158	2.8838
7	5-[10]-[10]-1	0.98212	0.6447	0.4157	3.3357
8	**5-[12]-[12]-1**	**0.99246**	**0.6472**	**0.4189**	**2.9616**
9	5-[14]-[14]-1	0.97245	0.6522	0.4254	2.6168

design and operational limits. These models help to develop communication with the raw data and transform them into a set of mathematical expressions which can be used for further processing.

Digital twin models can be generated through a range of methods from the area of multivariate statistics, machine learning, and artificial neural network. Research [42–44] has demonstrated that the neural network type of digital twin models can offer better statistical performance in terms of the prediction of the actual experimental or physical procedure. Thus, the application of an artificial neural network (ANN) with a multilayer perceptron (MLP) model is considered adequate for prediction purposes.

The applied MLP-ANN model in this article contains an input layer that contains 5 neurons corresponding to the five design variables, at least one hidden layer with a variable range of neurons, and an output layer that contains two neurons representing the two performance indicators. The computational procedure is applied through the development of an in-house code combined with the characteristics of the nftool box within the MATLAB interface. MLP-ANN works on the principle of backpropagation to minimize the mean-square error (MSE) calculated between the predicted performance indicator and the actual performance indicator. Three different backpropagation techniques are applied which include the Levenberg-Marquardt algorithm (LMA), Bayesian regularization algorithm (BRA), and Scaled Conjugate Gradient algorithm (SCGA). In this case, for both performance indicators, BRA came out to be the backpropagation technique with the highest statistical performance including Coefficient of Determination (R^2), Root-Mean-Square-Error (RMSE), MSE, and Mean-Absolute-Percentage-Error (MAPE). The experimental dataset was small and had a noisy behavior and literature has also shown that BRA is the most suitable for such a characteristic of the input data [45].

The functionality of MLP-ANN includes the process of multiplication of the neurons X_i from one layer with the appropriate weights w_{ik}, added with the bias b_{hk}, and goes through an activation function f_{sig}, written mathematically with: $f_{sig}\left(b_{hk} + \sum_{i=1}^{m} w_{ik} X_i\right)$. The output from the first layer is passed on to the second next layer until the final output can be obtained. Such an integrated process can be expressed using the mathematical expression: Performance indicator $= f_{sig}\left\{b_o + \sum_{k=1}^{h}\left[w_k \times f_{sig}\left(b_{hk} + \sum_{i=1}^{m} w_{ik} X_i\right)\right]\right\}$ [46]. The activation function is a tan-sigmoid of the form $\frac{2}{1+e^{-2p7}} - 1$. This mathematical procedure is applied in an iterative way using a BRA optimization algorithm to minimize the mean-

square-error and for the evaluation of weights and bias of each layer, and only 85% of the data is used for this training purposes whereas the remaining 15% of the data is used for the testing of final digital twin model. The 15% testing data has quite a significance because the trained model does not have any recognition for this testing data and an accurate prediction of this testing data set would determine the accurate prediction capability of the digital twin model.

Thus, it is understood that the generation of a suitable ANN architecture is an iterative procedure where the number of hidden layers, the number of neurons in each hidden layer, and the optimization technique should be iterated systematically. The results of such an iterative procedure are displayed in Table 3 for both cooling capacity and the total water footprints. The selection of the best architecture is based on the statistical performance indicators where it is desired to the maximum R^2, and minimum values of RMSE, MSE, and MAPE. The first four architectures for both performance indicators have only used one hidden layer having 6, 8, 10, and 20 neurons in it. The range of R^2 of such an architecture is from 0.97866 to 0.98744 for cooling capacity and 0.95821 to 0.97334 for the total water footprints. These values of R^2 are quite low because these digital twin models would be used for optimization purposes where the algorithm evaluates the model on its extremes and any lack of fit can yield an unreliable and unrealistic outcome. Thus, it is desired to obtain a relatively higher value of R^2. On the other side, an architecture with so many hidden neurons would also not be appropriate because it would be increasing the computational procedure. Thus, the ideal case is to find the architecture with the least number of hidden neurons.

As an alternative to this situation, multiple hidden layers are introduced in the iterative procedure which has yielded the development of a deep learning MLP-ANN model. As a rule of thumb, an architecture can be placed into the category of deep learning provided it has more than 4 layers including the input and the output layer. In this case, two hidden layers are introduced in which iterations are also conducted on the number of neurons in each hidden layer. For the cooling capacity, a total of 6, 8, and 10 hidden neurons are tested in each hidden layer, whereas, for the total water footprints, a total of 6, 8, 10, 12, and 14 hidden neurons are tested in each hidden layer. For the cooling capacity, it is noted that the R^2 has increased from 0.97866 to 0.98856 making a change of 1.01% by introducing a second hidden layer with the same number of neurons, in this case, 6. This is an appreciable change in R^2 because it has decreased the lack of fit in the regression model. However, as the number of neurons in the hidden layer is increased to 8 and 10, the performance of the predictive model has decreased which can be
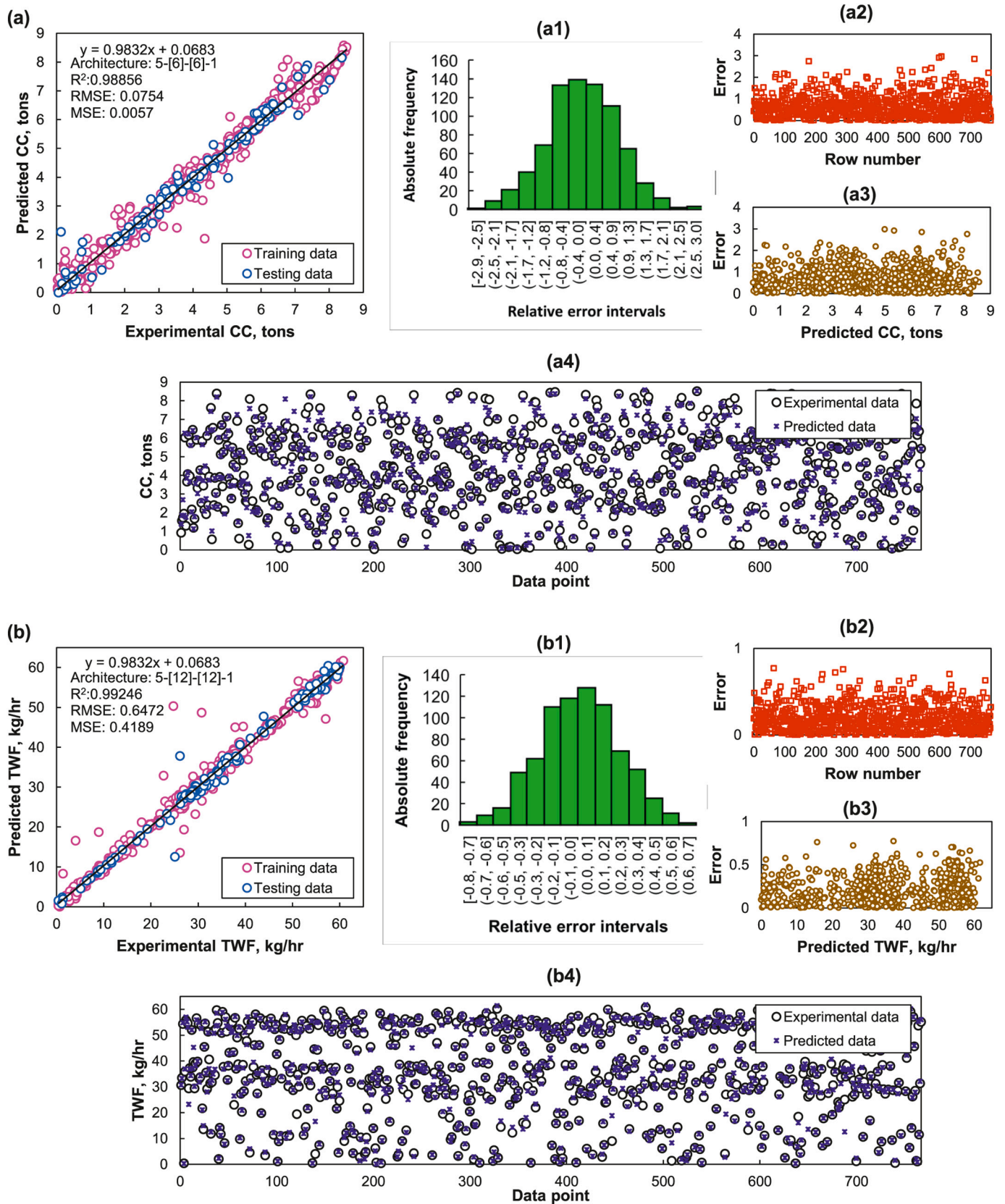
Fig. 3. (a and b) Linear statistical fit between the experimental data and the predicted data for the best architecture. Compliance of (a1 and b1) normality of errors, (a2 and b2) independence of errors, and (a3 and b3) homoscedasticity of errors. (a4 and b4) Response graph between the experimental and predicted data.
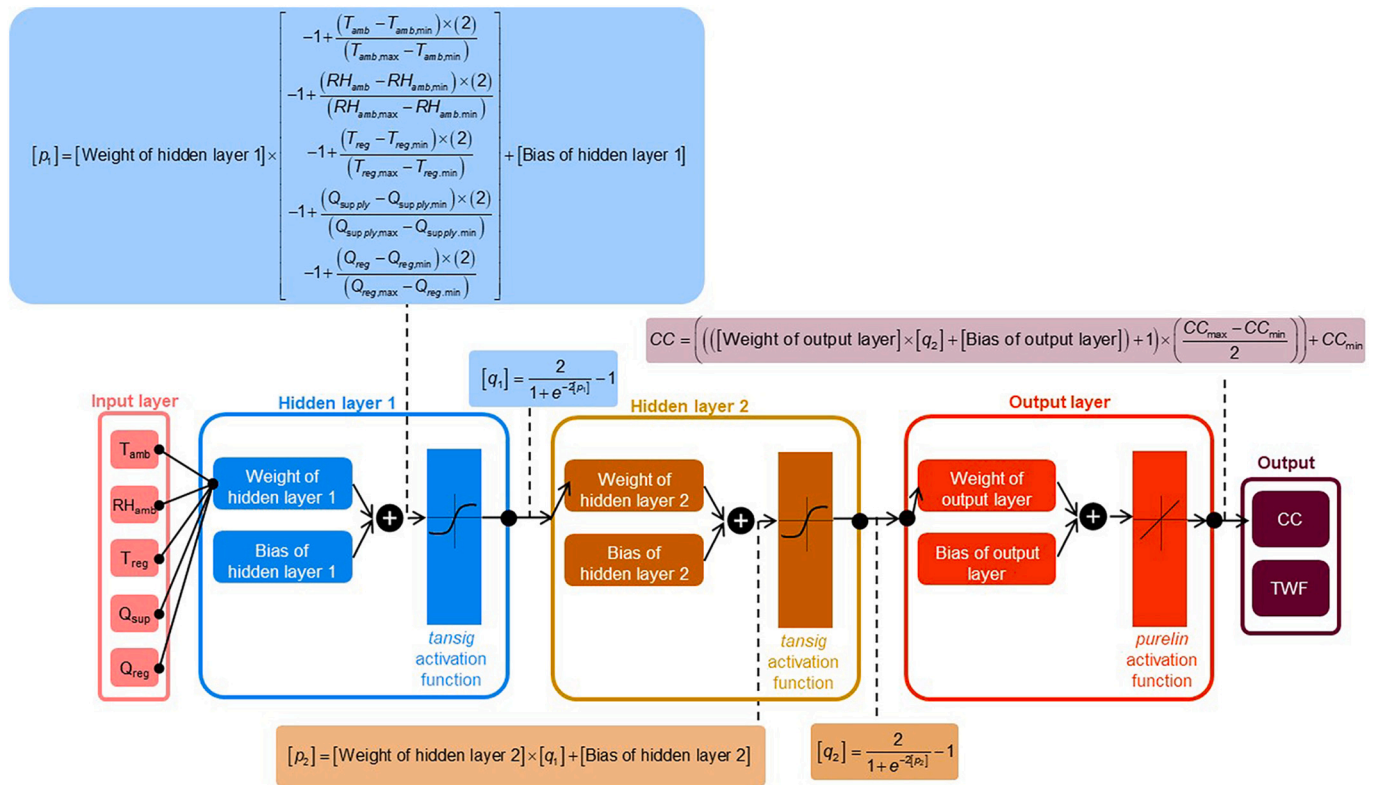
$$[p_1] = [\text{Weight of hidden layer 1}] \times \begin{bmatrix} -1 + \dfrac{(T_{amb} - T_{amb,min}) \times (2)}{(T_{amb,max} - T_{amb,min})} \\[2mm] -1 + \dfrac{(RH_{amb} - RH_{amb,min}) \times (2)}{(RH_{amb,max} - RH_{amb,min})} \\[2mm] -1 + \dfrac{(T_{reg} - T_{reg,min}) \times (2)}{(T_{reg,max} - T_{reg,min})} \\[2mm] -1 + \dfrac{(Q_{sup,ply} - Q_{sup,ply,min}) \times (2)}{(Q_{sup,ply,max} - Q_{supply,min})} \\[2mm] -1 + \dfrac{(Q_{reg} - Q_{reg,min}) \times (2)}{(Q_{reg,max} - Q_{reg,min})} \end{bmatrix} + [\text{Bias of hidden layer 1}]$$

$$CC = \left(\left(\left([\text{Weight of output layer}] \times [q_2] + [\text{Bias of output layer}] \right) + 1 \right) \times \left(\dfrac{CC_{max} - CC_{min}}{2} \right) \right) + CC_{min}$$

$$[q_1] = \dfrac{2}{1 + e^{-2[p_1]}} - 1$$

$$[p_2] = [\text{Weight of hidden layer 2}] \times [q_1] + [\text{Bias of hidden layer 2}]$$

$$[q_2] = \dfrac{2}{1 + e^{-2[p_2]}} - 1$$

Fig. 4. White-box model of artificial neural network for the estimation of performance indicator.

because of the mathematical complications resulting as an outcome of increasing the hidden neurons. In conclusion, the suitable architecture for the prediction of cooling capacity has two hidden layers with 6 neurons each, and the suitable architecture for the prediction of total water footprints has two hidden layers with 12 neurons each.

Once the optimal architecture is identified, the next step is to visualize its regressive performance which is done by plotting the experimental performance indicator concerning the predicted performance indicator. These results for the cooling capacity and total water footprints are displayed in Fig. 3. Ideally, the regressive fit between the actual and the predictive performance indicator should be linear with a unity slope and a zero y-intercept, but the real situation deviates a little from the ideality. In the case of cooling capacity and total water footprints, the value of the slope is 0.9832, whereas the bias is 0.0683 which are close to unity and zero, respectively. It is noted that the data distribution at the central part of both performance indicators has displayed a better regression fit as compared to its extremes which can be because of the unavailability of sufficient data after quartile 3 and before quartile 1. Fig. 3 (a4 and b4) displays another representation of the regressive fit in which both the predicted and the actual value are placed on the y-axis and the absolute difference between both can be noted clearly. This difference between the predicted and the actual value has quite a significance in the determination of the accuracy of fit and it is required that this error should comply with various assumptions of the regression procedure. It includes compliance with the assumptions like normality, independence, and homoscedasticity. The normality of the errors signifies the normal bell curve distribution of the errors which would comply with a universally acceptable distribution pattern. It can be verified by making a frequency diagram of the error terms as seen in Fig. 3 (a1 and b1). The independence of error tests the correlation between the design variables and their dependency. It is required that all the design variables should be independent otherwise, the regression fit might not be accurate. It is tested by plotting the residual errors with respect to the total number of data points. It is desired to have not any

definite visible pattern. In this case, as noted in Fig. 3 (a2 and b2), both performance indicators satisfy the assumption of independence of errors. Homoscedasticity is checked by plotting the error term with respect to the predicted performance indicator and this assumption is also verified as indicated in Fig. 3 (a3 and b3).

MLP-ANN-based digital twin models are useful because they can provide a direct empirical relationship between the design variables and the performance indicator. However, the current research has focused on a black-box or grey-box modeling approach where the in-depth explanation of this relationship is not declared properly. This brings difficulty in replication and validation studies in further research. Thus, it is necessary to add a white-box digital twin model with the application of the MLP-ANN model. Such a model is mathematically extensive but can provide an appropriate prediction of the performance indicator.

Such a white box is displayed graphically in Fig. 4. In the first step, all the variables are normalized using min-max constrained minimization between the range of −1 to +1 for effective implementation of the tan-sigmoid activation function. For example, the ambient temperature is normalized using: $-1 + \frac{(T_{amb} - T_{amb,min}) \times (2)}{(T_{amb,max} - T_{amb,min})}$ where 2 represents the difference between +1 to −1. All the design variables constitute five design variables of the input layer yielding a matrix having 1 column and 5 rows in which each row designates a different input design variable. This is multiplied by the weight matrix of the first hidden layer. As seen in eq. (5), the weight of the first hidden layer has 5 columns for 5 design variables and 6 rows for a total of 6 neurons in the first hidden layer applied in the case of cooling capacity. The bias vector (eq. (6)) of the first hidden layer is added to it. It yields a matrix $[p_1]$ that is used in the activation function yielding the matrix: $[q_1] = \frac{2}{1 + e^{-2[p_1]}} - 1$. This matrix $[q_1]$ is placed as an input to the next hidden layer and multiplied by its weight (see eq. (7)) and its bias (eq. (8)) which would result in the generation of the matrix $[p_2]$ going through the activation function and yielding $[q_2]$. Eventually, the same procedure is applied in the output layer using its weight and bias matrix which are presented in eqs.

(9) and (10), respectively. This would provide us with a normalized value of the cooling capacity which can be converted into its normal value by re-arranging the min-max normalization function as given in the equation: $CC = ((([\text{Weight of output layer}] \times [q_2] + [\text{Bias of output layer}]) + 1) \times (\frac{CC_{\max} - CC_{\min}}{2})) + CC_{\min}$.

counter-related. The cooling capacity is expected to maximize as the hot and dry air helps in the evaporation of more and more water. The system is therefore expected to maximize CC. However, in the case of TWF, minimization of water usage is desired. Therefore, the overall multi-objective function as shown in Eq. 11 is the minimization of –CC (or

$$[\text{Weight of hidden layer 1}] = \begin{bmatrix} 0.908123889431902 & -0.0542513491331009 & -1.64136579472561 & 0.351237943424630 & -0.251568025267574 \\ 2.12624802713820 & 1.67758315936998 & 1.80604726758061 & -1.29724404460463 & 0.362627157191961 \\ 1.35991930010710 & 0.272482859243860 & -2.52361330003952 & -1.75503929570321 & 1.34073448729706 \\ -0.509789974827116 & 1.71600475255588 & -1.20417828106988 & -2.98858550845512 & -2.45701783166648 \\ -0.576349479541600 & -3.15460539384414 & -0.601522171472399 & -4.96065581974215 & -1.90802783131018 \\ 4.09254097014555 & 4.15099580647972 & 1.35772654854594 & 1.62995236862397 & -0.243534565815890 \end{bmatrix} \quad (5)$$

maximization of CC) and TWF. Both are independent objectives; therefore a multi-objective function is presented.

While the constraints, put limits on the range of the quantification of both the functional parameters of CC and TWF. It is primarily the maximum and minimum ranges of the quantities as seen in the data sets and plotted in Fig. 2. This is the optimization of the objective function subject to constraints within the search space. In general, this is quite basic as the space entrains all the limit range of the independent pa-

$$[\text{Bias of hidden layer 1}] = \begin{bmatrix} -0.587639567850162 \\ -0.726473017497812 \\ 0.126891422414869 \\ 2.56860573655349 \\ 4.36557320159079 \\ -1.22263880866441 \end{bmatrix} \quad (6)$$

$$[\text{Weight of hidden layer 2}] = \begin{bmatrix} -0.527836384225245 & -0.591158257132058 & 0.323366594968683 & -0.371750441802957 & -1.10474202649740 & 0.271935210273667 \\ -1.13458153002614 & 2.49128898582503 & -0.231177186912914 & 2.73553786411625 & 0.651625847633708 & 0.914036569049580 \\ -1.25597702481848 & 1.34908271411628 & -1.45737327629581 & 4.08610302272680 & 1.84287122951395 & -0.287647170110649 \\ -0.983375593546844 & 2.15760468110013 & -0.117508275326039 & 3.24854532627833 & 0.612879230672708 & -0.634566678906166 \\ 1.18842430846094 & -0.0205898374321550 & -0.646738122413149 & -0.499519339205777 & -0.773745832907324 & -0.00484478967629552 \\ 2.80609809310152 & -0.240048492436197 & -0.0908927928052310 & 0.0512487763054620 & 0.167426555066086 & -0.0383573412843053 \end{bmatrix} \quad (7)$$

rameters as indicated in Fig. 2. However, keeping a blind eye on the parameters can easily lead to a local minimum which may not be a system performance indicator as the system behaves differently when outside conditions are well within the thermal comfort conditions as it is an open-air conditioning cycle.

This is a critical part of this work, the knowledge of the system dynamics is of utmost importance as the data-driven model and optimization are expected to lead to a non-operating system mode of working i. e., passing the outdoor air to comfort indoors without conditioning. This is an essential part of realistic decision-making and steps towards xAI

$$[\text{Bias of hidden layer 2}] = \begin{bmatrix} 0.0737795969181049 \\ -1.20473326037474 \\ 0.443419261116188 \\ 0.750968595338646 \\ 0.864395154696170 \\ -1.26905196849726 \end{bmatrix} \quad (8)$$

$$[\text{Bias of output layer}] = [-2.8608] \quad (9)$$

$$[\text{Weight of output layer}] = [-3.82317879725307 \quad -0.787910734258533 \\ -1.41511070491873 \quad 1.96965734854498 \quad 4.15790791801437 \quad -2.02482510392489] \quad (10)$$

4.3. Results of the applied optimization method

This section summarizes and discusses the optimization results. Starting with the objective function, as mentioned earlier, two outcome indicators are identified for this study including cooling capacity (CC) and total water footprint (TWF). In light of the discussion mentioned earlier and viewing the system as a block, both indicators are somewhat

(realizable artificial intelligence). This is the critical juncture in this work and points towards the fact that the intelligence in the data selection or its operating range is critical to evaluating the system performance as well as optimal conditions in multi-objective function optimization. For this reason and to realize the actual system performance instead of its by-pass operation (which is of importance when the control strategy of the whole building setup is analyzed), a curtailed range of independent parameters is used as search space as given in Eq. 11. It can be noticed that the space restricts the ambient temperature to a
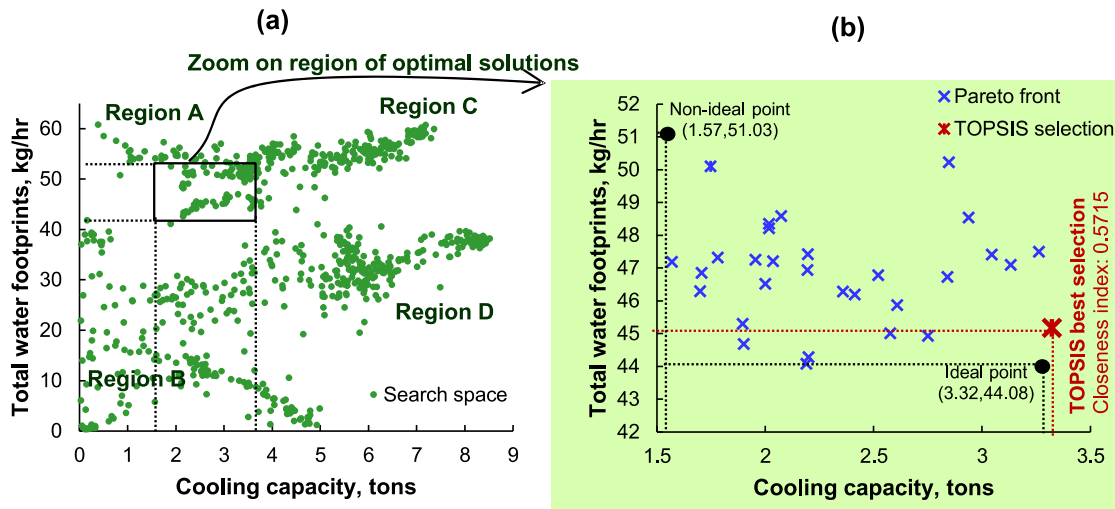
Fig. 5. (a) Search space of the data-driven optimization process, and (b) Pareto front along with TOPSIS best selection for final optimization results.

value at the borderline of thermal comfort, instead of a data-set based lowest value of ambient. Moreover, the relative ambient humidity is also limited to a lower bound of 50% (again a borderline value for thermal comfort).

$$\text{Objective function}: min\, f = \begin{cases} -CC \\ TWF \end{cases}$$

$$\text{Constraints}: \begin{cases} CC - 8.51 \le 0 \text{ and } -CC + 0.029 \le 0 \\ TWF - 60.78 \le 0 \text{ and } -TWF + 0.39 \le 0 \end{cases}$$

$$\text{Search space}: \begin{cases} 25^\circ C \le T_{amb} \le 36.76^\circ C \\ 50\% \le RH_{amb} \le 100\% \\ 30^\circ C \le T_{reg} \le 80.66^\circ C \\ 0.10 kg/s \le Q_{supply} \le 2.70 kg/s \\ 0.021 kg/s \le Q_{regeneration} \le 2.78 kg/s \end{cases} \quad (11)$$

The multi-objective function parameters of CC and TWF are shown in Fig. 5(a) for the search space and constraints as mentioned in Eq. 11. The range of variations of both parameters can be divided into certain quarters/regions. The four regions can be distinguished from the scatter observed in Fig. 5(a). Region A indicates the low CC regime with high TWF. Region B is at the bottom of the figure with low CC and TWF. Region C is opposite region B with high CC and high TWF. While region D is at a relatively lower TWF and high CC. One can note that the low TWF and higher CC are not seen in this scatter plot, the solution is most desirable and labeled as the Ideal solution. Each region has its own characteristics, as region A is dominated by high TWF while region B is low on the ability to cool the space at low CC. Region C is a relatively higher TWF as well as higher CC. It is imperative to notice that the ideal solution is the one with lower TWF and higher CC but distinguishing between these regions of Fig. 5(a); the merits of a certain region over

others are not plainly clear. Though region C is desirable in terms of CC but has the highest TWF. While region D is sparsely mapped in the scatter plot indicating that evaporative cooling has a significant role in air cooling and thus TWF shall happen to be significant in any case. Region B is not fulfilling the cooling demand and thus shall remain lower on CC as well as TWF. It seems that region A is somewhat more likely to have the optimal solution set and picking the right optimal conditions pertaining to closeness to the ideal solution is expected in the bordered region in Fig. 5(a). In fact, the Pareto front is zoomed in and shown in Fig. 5(b) for clarity. As region A is medium in terms of fulfilling CC requirements as well as lessening the TWF, the ideal solution remains (within region A) with the lowest TWF and highest CC i.e., towards the left bottom corner of Fig. 5(b). While the farthest point on the top left side of Fig. 5(b) is non-ideal with lower CC and higher TWF.

Using TOPSIS selection i.e., mapping the desirable solution closest to the ideal point is the optimal condition for this multi-objective optimization. The technique TOPSIS, which is an abbreviation of "The Technique for Order of Preference by Similarity to Ideal Solution", is a multicriteria decision-making algorithm to select the final optimal solution within the Pareto front. Since all the points on the Pareto front are optimal points, thus, such a multicriteria decision-making system is needed to give select one point within each optimal point. This technique is applied based upon a total of five steps called (a) normalization, (b) evaluation of ideal and non-ideal solutions, (c) calculation of positive

Table 4
The final optimal solution for optimal water resource consumption and cooling capacity.

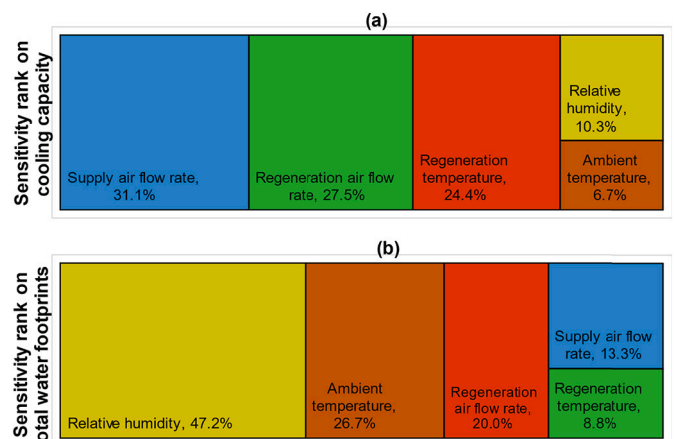| Variable	Symbol	Unit	Optimal value
Ambient temperature	T_{amb}	°C	28.0
Ambient relative humidity	RH_{amb}	%	52.0
Regeneration temperature	T_{reg}	°C	70.0
Supply flow rate	Q_{supply}	kg/s	2.13
Regeneration flow rate	$Q_{regeneration}$	kg/s	2.35
Cooling capacity	CC	tons	3.32
Total water footprints	TWF	kg/h	45.17

Fig. 6. Sensitivity of the design variables on the (a) cooling capacity, and (b) total water footprints.

and negative Euclidian distances, (d) calculation of relative closeness index, and (e) sorting. In the first step, the normalization of all the vectors (decision/design variables, and fitness/performance indicators) is accomplished through the Euclidian non-dimensioning method. The ideal and non-ideal points are evaluated which are in reality some hypothetical points in the design problem but can help us to identify the best candidate within the TOPSIS selection. The ideal point (desired conditions) for this optimization problem would be the maximum value of cooling capacity and the minimum value of the total water footprints within the vector of a fitness function. On the other side, the non-ideal point (non-desired conditions) for the subject case would be the minimum cooling capacity with the maximum total water footprints. Once, the ideal and the non-ideal points are identified, then positive and negative Euclidian distances are calculated for each optimal point of the Pareto front with respect to the ideal and non-ideal solutions. These distances are used to evaluate the relative closeness index which is defined as the relative geometrical closeness of any Pareto front point with respect to the ideal solution. Thus, sorting the matrix of relative closeness index and its highest value is the realistic optimal point on the Pareto front. Further technical details of its implementation along with the relative equations can be consulted from Tariq et al. [42,43] and Tzuc et al. [47].

The selected point, in terms of nearness to the ideal point and farthest from the non-ideal point, corresponds to the input and output parameters listed in Table 4. It is clear that the system has the optimal conditions in relatively calmer ambient conditions where the ambient temperature is around 28 °C at a relative humidity of 52%. At these conditions, the system cooling capacity is more than 3 tons with more than 45 kg of water usage in one hour at the listed flow rates. It is very important to mention that the system shall be operational at higher ambient temperature and relative humidity, however, it shall be getting far from the ideal point as mentioned in Fig. 5(b). One may appreciate that the hot and dry water is expected to drain the water resource, while high ambient humidity is expected to increase the desiccant wheel load in terms of frequent recharging.

4.4. Sensitivity analysis

The sensitivity analysis is evaluated using the Garson method which takes the synaptic weights of the input, hidden, and output layers (eqs. 5–10). It is based upon the analogy that the magnitude of the weight of each variable would eventually indicate the strength of the corresponding variable on the fitness function. Thus, for each fitness function, the Garson method is applied two times to give the resulting sensitivity ranks. Further theory, implementation, and relative mathematics of the Garson method can be consulted by Ajbar et al. [48].

The overall impact of the above analysis can be more appreciated with the help of the relative impact each of the operating parameters is causing on the overall multi-objective function. This is analyzed here in this section that the considered input/independent parameters are influencing the desired outcomes. Amongst the considered 05 independent parameters, each of these is analyzed for the output parameters for CC and TWF in Fig. 6(a) and (b) respectively.

Clearly, the ambient temperature and relative humidity are less influential on the cooling capacity as indicated by the sensitivity analysis shown in Fig. 6(a). The most important factor is the supply airflow rate and the return/regenerative flow of air along with the regenerative temperature. Clearly, the higher need for airflow and regeneration requirements impact the cooling capacity of the system. While the ambient air conditions are somewhat less important as the intermediate components in the system damp the direct impact of ambient air on the system.

While the total water footprint is primarily driven by the ambient air condition and especially the number of water vapors carried by the ambient air while entering the system. This is counter to the characteristics of CC and thus explains the challenge faced in this multi-

objective optimization problem. Quite clearly, the independent parameters have their own impacts on the system; however, the combined influence is what the multi-objective optimization is able to evaluate and present.

5. Conclusions

Desiccant evaporative cooling systems are energetically, economically, and environmentally favorable candidates to handle the air conditioning load in commercial and residential buildings subjected to a specific range of climatic conditions. Its prime limitation is related to its high water footprint which is required to produce the required cooling capacity. Especially with the novel technologies like the usage of the Maisotsenko Cycle, the potential of desiccant-enhanced indirect evaporative coolers is more suitable, but it is primarily constrained by its high water usage too. This work is dedicated to applying a methodological framework including deep learning, genetic algorithm, and multicriteria decision-making analysis to reduce the water footprints of the desiccant-enhanced evaporative coolers with experimental data obtained using real building conditions. The objective is to display a multicriteria outcome which also includes the maximization of the cooling capacity too. The following are the main conclusions obtained from this research:

1. The application of an artificial neural network with a deep learning architecture using the Bayesian Regularization algorithm to optimize the bias and weights offers the best statistical performance.
2. A deep learning algorithm with architecture 5-[6]-[6]-1 is optimal to predict the experimental data set of cooling capacity and offers a coefficient of determination of 0.98856, along with RMSE: 0.0754, MSE: 0.0057, and MAPE: 0.0290.
3. A deep learning algorithm with architecture 5-[12]-[12]-1 is optimal to predict the experimental data set of total water footprints and offers a coefficient of determination of 0.99246, along with RMSE: 0.6472, MSE: 0.4189, and MAPE: 2.9616.
4. Non-sorting genetic algorithm (NSGA-II) and multicriteria decision analysis using TOPSIS have suggested that the optimized total water footprints are 45.17 kg/h with a system of 3.32 tons of refrigeration. These optimal values are found in the best combination of design variables in which the ambient temperature is 28 °C, ambient relative humidity is 52.0%, supply airflow rate is 2.13 kg/s, and regeneration flow rate is 2.35 kg/s, and the regeneration temperature is 70.0 °C.
5. Sensitivity analysis has suggested that the supply airflow rate and regeneration airflow rate are the most dominant design variables for the cooling capacity, whereas the relative humidity and the ambient temperature are the most dominant for the evaluation of total water footprints.

CRediT authorship contribution statement

Rasikh Tariq: Methodology, Software, Validation, Formal analysis, Investigation, Data curation, Writing – original draft, Writing – review & editing, Visualization. **Muzaffar Ali:** Conceptualization, Methodology, Validation, Investigation, Resources, Writing – original draft, Writing – review & editing, Visualization, Supervision, Project administration, Funding acquisition. **Nadeem Ahmed Sheikh:** Conceptualization, Methodology, Validation, Investigation, Resources, Writing – original draft, Writing – review & editing, Visualization, Supervision, Project administration, Funding acquisition. **Muhammad Wakil Shahzad:** Supervision, Project administration, Funding acquisition, Writing – review & editing, Investigation. **Ben Bin Xu:** Writing – review & editing, Investigation.

Declaration of Competing Interest

The authors declare that they have no known competing financial interests or personal relationships that could have appeared to influence the work reported in this paper.

Data availability

Data will be made available on request.

Acknowledgment

References

[1] O.A. Alawi, N.A.C. Sidik, M. Beriache, Applications of nanorefrigerant and nanolubricants in refrigeration, air-conditioning and heat pump systems: a review, Int. Commun. Heat Mass Transf. 68 (2015) 91–97, https://doi.org/10.1016/J.ICHEATMASSTRANSFER.2015.08.014.

[2] M.A. Al-Nimr, M.R. Daqqaq, M.A. Hader, Effect of working fluids on the performance of a novel summer air conditioning system, Int. Commun. Heat Mass Transf. 28 (2001) 565–573, https://doi.org/10.1016/S0735-1933(01)00261-5.

[3] K.N. Çerçi, E. Hürdoğan, Comparative study of multiple linear regression (MLR) and artificial neural network (ANN) techniques to model a solid desiccant wheel, Int. Commun. Heat Mass Transf. 116 (2020), 104713, https://doi.org/10.1016/J.ICHEATMASSTRANSFER.2020.104713.

[4] U. Sajjad, N. Abbas, K. Hamid, S. Abbas, I. Hussain, S.M. Ammar, M. Sultan, H.M. Ali, M. Hussain, T. Ur Rehman, C.C. Wang, A review of recent advances in indirect evaporative cooling technology, Int. Commun. Heat Mass Transf. 122 (2021), 105140, https://doi.org/10.1016/J.ICHEATMASSTRANSFER.2021.105140.

[5] C. Kian Jon, M.R. Islam, N. Kim Choon, M.W. Shahzad, Dissipative Losses in Cooling Cycles, 2021, https://doi.org/10.1007/978-981-15-8477-0_7.

[6] K.C. Ng, M.W. Shahzad, M. Burhan, S.J. Oh, Approaches to energy efficiency in air conditioning: innovative processes and thermodynamics, Energy Procedia (2019), https://doi.org/10.1016/j.egypro.2019.01.349.

[7] Q. Chen, M. Kum Ja, M. Burhan, F.H. Akhtar, M.W. Shahzad, D. Ybyraiymkul, K.C. Ng, A hybrid indirect evaporative cooling-mechanical vapor compression process for energy-efficient air conditioning, Energy Convers. Manag. 248 (2021), 114798, https://doi.org/10.1016/j.enconman.2021.114798.

[8] M.W. Shahzad, M. Burhan, D. Ybyraiymkul, S.J. Oh, K.C. Ng, An improved indirect evaporative cooler experimental investigation, Appl. Energy 256 (2019) 113934, https://doi.org/10.1016/j.apenergy.2019.113934.

[9] M.W. Shahzad, J. Lin, B. Bin Xu, L. Dala, Q. Chen, M. Burhan, M. Sultan, W. Worek, K.C. Ng, A spatiotemporal indirect evaporative cooler enabled by transiently interceding water mist, Energy. 217 (2021), 119352, https://doi.org/10.1016/j.energy.2020.119352.

[10] J. Lin, K. Thu, S. Karthik, M.W. Shahzad, R. Wang, K.J. Chua, Understanding the transient behavior of the dew point evaporative cooler from the first and second law of thermodynamics, Energy Convers. Manag. 244 (2021), 114471, https://doi.org/10.1016/j.enconman.2021.114471.

[11] J. Lin, M.W. Shahzad, J. Li, J. Long, C. Li, K.J. Chua, A robust physics-based model framework of the dew point evaporative cooler: from fundamentals to applications, Energy Convers. Manag. 233 (2021), 113925, https://doi.org/10.1016/j.enconman.2021.113925.

[12] D. Pandelidis, A. Cichoń, A. Pacak, P. Drąg, M. Drąg, W. Worek, S. Cetin, Performance study of the cross-flow Maisotsenko cycle in humid climate conditions, Int. Commun. Heat Mass Transf. 115 (2020), 104581, https://doi.org/10.1016/j.icheatmasstransfer.2020.104581.

[13] R. Prommas, P. Rattanadecho, D. Cholaseuk, Energy and exergy analyses in drying process of porous media using hot air, Int. Commun. Heat Mass Transf. 37 (2010) 372–378, https://doi.org/10.1016/J.ICHEATMASSTRANSFER.2009.12.006.

[14] E.M. Salilih, N.H. Abu-Hamdeh, H.F. Oztop, Analysis of double U-tube ground heat exchanger for renewable energy applications with two-region simulation model by combining analytical and numerical techniques, Int. Commun. Heat Mass Transf.

[15] C. Tang, K. Vafai, C. Gu, K.N. Gloria, M.D.R. Karim, Experimental investigation of dehumidification performance of a vapor compression refrigeration system, Int. Commun. Heat Mass Transf. 137 (2022), 106282, https://doi.org/10.1016/J.ICHEATMASSTRANSFER.2022.106282.

[16] X. Shi, Y. Mu, G. Chen, X. Zhang, Experimental investigation on the start-up characteristics of single loop thermosyphon for motorized spindle bearing-shaft system cooling, Int. Commun. Heat Mass Transf. 120 (2021), 104989, https://doi.org/10.1016/J.ICHEATMASSTRANSFER.2020.104989.

[17] S.E. Rafiee, Experimental and thermo-dynamical analysis of fully turbulent gas flows in vortex tube- fluid, temperature and power separations, isentropic efficiency, coefficient of performance (COP), Int. Commun. Heat Mass Transf. 138 (2022), 106296, https://doi.org/10.1016/J.ICHEATMASSTRANSFER.2022.106296.

[18] J. Mohammadpour, S. Husain, F. Salehi, A. Lee, Machine learning regression-CFD models for the nanofluid heat transfer of a microchannel heat sink with double synthetic jets, Int. Commun. Heat Mass Transf. 130 (2022), 105808, https://doi.org/10.1016/J.ICHEATMASSTRANSFER.2021.105808.

[19] J.X. Wang, Z. Wu, M.L. Zhong, S. Yao, Data-driven modeling of a forced convection system for super-real-time transient thermal performance prediction, Int. Commun. Heat Mass Transf. 126 (2021), 105387, https://doi.org/10.1016/J.ICHEATMASSTRANSFER.2021.105387.

[20] D. Kim, J. Lee, S. Do, P.J. Mago, K.H. Lee, H. Cho, Energy modeling and model predictive control for HVAC in buildings: a review of current research trends, Energies 15 (2022), https://doi.org/10.3390/EN15197231. Page 7231. 15 (2022) 7231.

[21] D.B. Jani, M. Mishra, P.K. Sahoo, Application of artificial neural network for predicting performance of solid desiccant cooling systems – a review, Renew. Sust. Energ. Rev. 80 (2017) 352–366, https://doi.org/10.1016/J.RSER.2017.05.169.

[22] M.H. Demir, S. Cetin, O. Haggag, H.G. Demir, W. Worek, J. Premer, D. Pandelidis, Independent temperature and humidity control of a precooled desiccant air cooling system with proportional and fuzzy logic + proportional based controllers, Int. Commun. Heat Mass Transf. 139 (2022), 106451, https://doi.org/10.1016/J.ICHEATMASSTRANSFER.2022.106451.

[23] Y. Chen, H. Yan, H. Yang, Comparative study of on-off control and novel high-low control of regenerative indirect evaporative cooler (RIEC), Appl. Energy 225 (2018) 233–243, https://doi.org/10.1016/J.APENERGY.2018.05.046.

[24] H. Yan, Y. Chen, W. Zhang, Year-round-based optimization of high-low control in the regenerative indirect evaporative cooler (RIEC), Doi:10.1080/23744731.2019.1620576 25 (2019) 1394–1405, https://doi.org/10.1080/23744731.2019.1620576.

[25] Y. Chen, H. Yan, Y. Luo, H. Yang, A proportional–integral (PI) law based variable speed technology for temperature control in indirect evaporative cooling system, Appl. Energy 251 (2019), 113390, https://doi.org/10.1016/J.APENERGY.2019.113390.

[26] Y.E. Güzelel, U. Olmuş, K.N. Çerçi, O. Büyükalaca, New multiple regression and machine learning models of rotary desiccant wheel for unbalanced flow conditions, Int. Commun. Heat Mass Transf. 134 (2022), 106006, https://doi.org/10.1016/J.ICHEATMASSTRANSFER.2022.106006.

[27] G. Priyadarshi, D. Baruah, B. Kiran Naik, Design and performance prediction of desiccant coated heat exchanger using ANFIS–AI tool and dynamic model, Appl. Therm. Eng. 217 (2022), 119034, https://doi.org/10.1016/J.APPLTHERMALENG.2022.119034.

[28] M. Goldsworthy, S. White, Optimisation of a desiccant cooling system design with indirect evaporative cooler, Int. J. Refrig. 34 (2011) 148–158, https://doi.org/10.1016/J.IJREFRIG.2010.07.005.

[29] H.-Y. Tsai, C.-T. Wu, Optimization of a rotary desiccant wheel for enthalpy recovery of air-conditioning in a humid hospitality environment, Heliyon. 8 (2022), e10796, https://doi.org/10.1016/J.HELIYON.2022.E10796.

[30] S. Wang, R. Tu, Q. Zhang, Dynamic performance analyses and optimization studies on air dehumidifiers using multi-stage desiccant plates, Appl. Therm. Eng. 212 (2022), 118546, https://doi.org/10.1016/J.APPLTHERMALENG.2022.118546.

[31] S. Rayegan, S. Motaghian, G. Heidarinejad, H. Pasdarshahri, P. Ahmadi, M.A. Rosen, Dynamic simulation and multi-objective optimization of a solar-assisted desiccant cooling system integrated with ground source renewable energy, Appl. Therm. Eng. 173 (2020), 115210, https://doi.org/10.1016/J.APPLTHERMALENG.2020.115210.

[32] Q. Zhang, X. Liu, T. Zhang, Y. Xie, Performance optimization of a heat pump driven liquid desiccant dehumidification system using exergy analysis, Energy. 204 (2020), 117891, https://doi.org/10.1016/J.ENERGY.2020.117891.

[33] X. Ou, W. Cai, X. He, Model-based optimization strategy for a liquid desiccant cooling and dehumidification system, Energy Build. 194 (2019) 21–32, https://doi.org/10.1016/J.ENBUILD.2019.04.019.

[34] R. Tu, J. Li, Y. Hwang, Fresh air humidification in winter using desiccant wheels for cold and dry climate regions: optimization study of humidification processes, Int. J. Refrig. 118 (2020) 121–130, https://doi.org/10.1016/J.IJREFRIG.2020.04.009.

[35] A.F. Boudjabi, C. Maalouf, T. Moussa, D. Abada, D. Rouag, M. Lachi, G. Polidori, Analysis and multi-response optimization of two dew point cooler configurations using the desirability function approach, Energy Rep. 7 (2021) 5289–5304, https://doi.org/10.1016/J.EGYR.2021.08.128.

[36] S. Motaghian, H. Pasdarshahri, Regeneration energy analysis and optimization in desiccant wheels using purge mechanism, J. Build. Eng. 27 (2020), 100980, https://doi.org/10.1016/J.JOBE.2019.100980.

[37] Y. Chen, Y. Liu, D. Wang, X. Luo, J.J.J. Liu, J.J.J. Liu, Y. Wang, J.J.J. Liu, Performance and optimization of a novel solar-driven liquid desiccant air

conditioning system suitable for extremely hot and humid climates, Energy Convers. Manag. 215 (2020), 112899, https://doi.org/10.1016/J. ENCONMAN.2020.112899.

[38] A. Bouchaala, O. Merroun, A. Sakim, A MOPSO algorithm based on pareto dominance concept for comprehensive analysis of a conventional adsorption desiccant cooling system, J. Build. Eng. 60 (2022), 105189, https://doi.org/ 10.1016/J.JOBE.2022.105189.

[39] P. Shamsizadeh, E. Afshari, Numerical modeling of a membrane humidifier for mechanical ventilation, Int. Commun. Heat Mass Transf. 132 (2022), 105931, https://doi.org/10.1016/J.ICHEATMASSTRANSFER.2022.105931.

[40] A.K. Sleiti, J.S. Kapat, L. Vesely, Digital twin in energy industry: proposed robust digital twin for power plant and other complex capital-intensive large engineering systems, Energy Rep. 8 (2022) 3704–3726, https://doi.org/10.1016/J. EGYR.2022.02.305.

[41] M. Ali, V. Vukovic, N.A. Sheikh, H.M. Ali, M.H. Sahir, Enhancement and integration of desiccant evaporative cooling system model calibrated and validated under transient operating conditions, Appl. Therm. Eng. 75 (2015) 1093–1105, https://doi.org/10.1016/j.applthermaleng.2014.10.064.

[42] R. Tariq, C.E. Torres-Aguilar, J. Xamán, I. Zavala-Guillén, A. Bassam, L.J. Ricalde, O. Carvente, Digital twin models for optimization and global projection of building-integrated solar chimney, Build. Environ. (2022), 108807, https://doi. org/10.1016/J.BUILDENV.2022.108807.

[43] R. Tariq, C.E.E. Torres-Aguilar, N.A. Sheikh, T. Ahmad, J. Xamán, A. Bassam, Data engineering for digital twining and optimization of naturally ventilated solar

façade with phase changing material under global projection scenarios, Renew. Energy 187 (2022) 1184–1203, https://doi.org/10.1016/j.renene.2022.01.044.

[44] R. Tariq, Y. Hussain, N.A. Sheikh, K. Afaq, H.M. Ali, Regression-based empirical modeling of thermal conductivity of CuO-water Nanofluid using data-driven techniques, Int. J. Thermophys. 41 (2020), https://doi.org/10.1007/s10765-020-2619-9.

[45] R. Tariq, A.J. Cetina-Quiñones, V. Cardoso-Fernández, H.-L. Daniela-Abigail, B. Soberanis, M.A. Escalante, M.V. De Lille, Artificial intelligence assisted technoeconomic optimization scenarios of hybrid energy systems for water management of an isolated community, Sustain. Energy Technol. Assessments. (2021) 1–24.

[46] A.I. Lawal, An artificial neural network-based mathematical model for the prediction of blast-induced ground vibration in granite quarries in Ibadan, Oyo State, Nigeria, Sci. African. 8 (2020), e00413, https://doi.org/10.1016/j. sciaf.2020.e00413.

[47] O. May Tzuc, A. Bassam, L.J. Ricalde, O.A. Jaramillo, M. Flota-Bañuelos, M. A. Escalante Soberanis, Environmental-economic optimization for implementation of parabolic collectors in the industrial process heat generation: case study of Mexico, J. Clean. Prod. 242 (2020), 118538, https://doi.org/10.1016/j. jclepro.2019.118538.

[48] W. Ajbar, A. Parrales, U. Cruz-Jacobo, R.A. Conde-Gutiérrez, A. Bassam, O. A. Jaramillo, J.A. Hernández, The multivariable inverse artificial neural network combined with GA and PSO to improve the performance of solar parabolic trough collector, Appl. Therm. Eng. 189 (2021), 116651, https://doi.org/10.1016/J. APPLTHERMALENG.2021.116651.